Research Article

Sören Laubach*, Gerd Ehret, Jörg Riebeling and Peter Lehmann

A new form measurement system based on subaperture stitching with a line-scanning interferometer

DOI 10.1515/aot-2016-0039
Received June 21, 2016; accepted August 19, 2016; previously published online October 5, 2016

Abstract: A new optical form measurement system for almost rotational symmetric surfaces has been set up. It is based on an interferometric line sensor applying sinusoidal path length modulation in combination with a movement system. With this system, ring-shaped subapertures of the specimens are measured. The system is especially suitable for measuring spheres and aspheres with a broad range of radii (r > 50 mm). The individual subapertures are stitched together to yield the full 3D topography. Because the rotation of the specimen by more than 360° has to yield the same results, inherent consistency tests are possible. Example measurements of a sphere are shown and discussed. Reproducibility measurements for one ring scan performed with the system show a standard deviation of 14 nm. The system can be set up at a moderate price as off-the-shelf mechanical and optoelectronic devices can be used. Future improvements of the system are discussed.

Keywords: form measurement; interferometry; metrology.

1 Introduction

For the measurement of the surface form of precision-machined components, numerous approaches are known [1], which can be classified into tactile and optical methods.

***Corresponding author: Sören Laubach,** Physikalisch-Technische Bundesanstalt, Bundesallee 100, 38116 Braunschweig, Germany, e-mail: soeren.laubach@ptb.de
Gerd Ehret: Physikalisch-Technische Bundesanstalt, Bundesallee 100, 38116 Braunschweig, Germany
Jörg Riebeling and Peter Lehmann: Department of Electrical Engineering, University of Kassel, Wilhelmshöher Allee 71, 34121 Kassel, Germany

www.degruyter.com/aot
© 2016 THOSS Media and De Gruyter

Tactile and also pointwise optical measurement techniques typically have slow measurement speeds because they have to scan the 2D surface point-by-point. Consequently, the accuracy achieved with these pointwise measuring systems directly relies on the accuracy of the movement system, thus enabling absolute form measurements. Tactile sensors have the advantage that the interaction of the mechanical probing system with the specimen can be modeled very well [2], but they generally run the risk of damaging the measured surface [3]. Tactile methods also have the capability to measure a very broad range of surface forms. Optical pointwise measurement systems use, for example, chromatic-confocal sensors or interferometric sensors using multiwavelength methods and may accomplish large height measurement ranges, which facilitate a fast measurement of one dimension without mechanical movement. Furthermore, as long as the point sensor is normal to the specimen's surface, nearly every form can be measured [4].

Instantaneous 2D form measurement systems using optical interferometry enable fast measurements. The application range of these systems is restricted by the form of the surface under investigation, for example, due to large surface height variations. Various methods (e.g. phase-shifting or white-light interferometry) are applied in various well-used instruments [5, 6]. Advanced techniques such as single-shot phase-shifting methods [7] produce instantaneous four phase-shifted images that are acquired by a single camera. Due to the single-shot technique, the system is very robust against mechanical disturbances. Instead of recording the phase-shifted interferograms simultaneously with the same image sensor [8], also several image sensors can be used [9], resulting in higher lateral resolution. For larger specimens, subaperture stitching methods are in use. A commercially available system using subaperture stitching combines flexibility and interferometric accuracy [10]. This system tilts the specimen with respect to the sensor to ensure that the fringe density stays in a reasonable range.

To combine the advantages of pointwise methods (less restrictions to the surface under test) and areal methods (fast measurements), we developed a system with an interferometric line sensor that tracks the contour of the specimen [11]. This approach reduces the measurement time compared to tactile or pointwise optical techniques as a large number of sensors measure simultaneously. To enhance the measurement speed further, we use an oscillating reference surface [12–14], thus realizing a sinusoidal path length modulation, a technique described previously by Sasaki et al. [15, 16]. Other techniques using so-called carrier fringe methods require the specimen to be tilted with respect to the sensor [17]. The presented set-up does not require this tilting; thus, retrace errors can be neglected. In comparison to 2D sensors, the line sensor can be aligned better to the specimen's geometry, thus enabling the measurement of more complex surface forms such as steep aspheres.

In this paper, we present the set-up of the system and a model including the significant error influences. The measurement procedure for rotational symmetric specimens with the evaluation of the measured data, including the stitching process, is explained. In addition, we present some measurement examples regarding stability, reproducibility, and the resolution of the system. Finally, we show subaperture measurements that are stitched to a complete 3D topography and give an outlook on further improvements.

2 Set-up of the line-scanning interferometer

The line-scanning interferometer is based on a Michelson interferometer configuration with an oscillating reference mirror. The light source consists of a green LED in combination with a narrowband interference filter to enlarge the coherence length and thus to increase the height measurement range (center wavelength: 525 nm, coherence length: about 18 μm). The light is collimated, so that the reference mirror and the specimen are illuminated with a nearly plane wavefront. The interference pattern is imaged and captured by the line-scan camera using long-distance microscope objectives with different magnifications (see Figure 1A). The typically used infinity-corrected 5× microscope objective has a numerical aperture of 0.14 and a working distance of 34 mm. With this configuration,

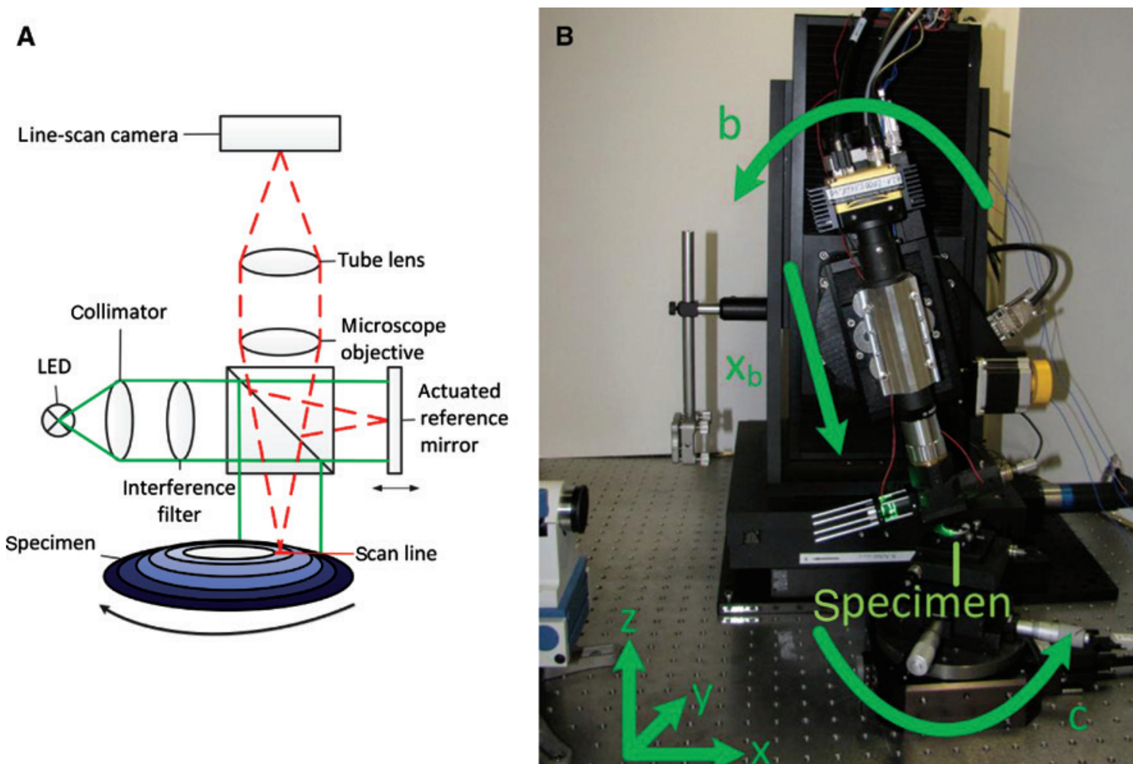

Figure 1: (A) Schematic diagram of the line-scanning interferometer with the actuated reference mirror. Solid line, illumination path; dashed line, imaging path. (B) The sensor is mounted on a five-axis movement system, and the specimen is adjusted manually and rotated with a rotation stage.

the camera line corresponds to a line of 2 mm length on the specimen. The system is optimized for measuring surfaces with a diameter of 25.4 mm. In the current set-up, the minimum radius of curvature is about 50 mm and is given by the limited coherence length in combination with the maximum microscope magnification.

The line sensor is mounted on a five-axis movement system, while the specimen is fixed on a rotational table with the rotation axis c below the sensor. A manual xy stage in combination with a tip/tilt unit is mounted on this c-axis to align the specimen with respect to the rotation axis c. The sensor has to be displaced to track the contour of the specimen and avoid fringe densities that are too high. Depending on whether the specimen is a plane mirror, a concave sphere/asphere, or a convex sphere/asphere, these axes are used in different ways to track the sensor relative to the specimen (see Figure 1B).

The resolution in the scanning direction depends on the scanning speed, for example, when using a typical scanning speed of 10°/s, and then about 15 000 height values are measured for each pixel for a complete subaperture ring. The measurement time is about half a minute and the evaluation takes a few minutes.

3 Modeling of the system

The system needs to be modeled to identify, quantify, and possibly correct the influence of parameters that affect the measurement result and measurement uncertainty. Besides this, the modeling of the measurement system is also useful to decide whether a specimen is measurable or not. In the following, we will present the model and especially discuss results with specific regard to the uncertainty of the particular system. To simplify the model, we first discuss parameters that have only minor influence.

Input quantities such as temperature, pressure, and humidity are expected to be negligible because one ring scan takes only a few seconds and a whole 25.4 mm topography can be measured in a few minutes plus some additional time that is necessary to move the interferometer in the x-direction and tilt the sensor. The effects of positioning errors of the movement axes can be partially corrected by the stitching process. Parameters that have major effects on the measurement are tilt errors of the specimen, rotation errors of the rotational c-axis, and measurement noise stemming from the electronic sensor and mechanical vibrations.

The interference intensity $I(t)$ can be described by Eq. (1). I_{Off} is the offset intensity, I_{Amp} is the amplitude of the interference fringes, $z(t)$ is the movement of the reference mirror and $\varphi(t)$ denotes the phase change. The phase term $\varphi(t)$ includes the topography z_{topo}, which is to be measured, in addition to other quantities such as possible tilts of the specimen with respect to the optical axis, possible tilt error motions, or unavoidable electronic and environmental vibration noise. A tilt of the specimen with respect to the optical axis is due to residual alignment errors, which leads to a wobbling motion during rotation of the specimen. To describe this effect, a sinusoidal height modulation with an amplitude A_{tilt} and a frequency that is equal to the rotation frequency is added to the phase of the signal [φ_{tilt}; see Eq. (2)]. The rotation frequency is proportional to $1/N_{\text{meas}}$, where N_{meas} is the number of height values measured during a full rotation of the specimen. In addition, rotation errors of the rotating table exist, which can be described by a sinusoidal phase modulation $\varphi_{\text{motion}_{\text{error}}}$ with an amplitude $A_{\text{motion}_{\text{error}}}$ and a frequency of the rotation frequency. This is done to keep the model as simple as possible; to get a more accurate model, more harmonics have to be taken into account. To describe the influences due to environmental noise, a random, normally distributed phase φ_{noise} is added.

The systematic effects can be calibrated by a reference flat and can thus be minimized. The measurement uncertainty and the measurement time of course scale up with the specimen diameter.

$$I(t)=I_{\text{Off}}+I_{\text{Amp}}\times\cos\left(\frac{4\cdot\pi}{\lambda}\cdot z(t)+\varphi(t)\right) \tag{1}$$

$$\begin{aligned}\varphi(t)&=\varphi_{\text{topo}}+\varphi_{\text{tilt}}+\varphi_{\text{motion}_{\text{error}}}+\varphi_{\text{noise}}\\&=\frac{4\cdot\pi}{\lambda}\cdot\left[z_{\text{topo}}(\varphi_{\text{motion}})+A_{\text{tilt}}\cdot\sin\left(\frac{2\cdot\pi}{N_{\text{meas}}}\cdot\varphi_{\text{motion}}\right)\right.\\&\left.+\ldots A_{\text{motion}_{\text{error}}}\cdot\sin\left(\frac{2\cdot\pi}{N_{\text{meas}}}\cdot\varphi_{\text{motion}}\right)\right]+\varphi_{\text{noise}}\end{aligned} \tag{2}$$

Figure 2 shows the simulation results for a convex specimen using two different microscope magnifications. Two assumptions were made: it is supposed that the measurement object is illuminated with a plane wavefront and that the interferometer is well aligned with respect to the surface of the specimen, that is, the center of the camera line images the local maximum of the surface topography. Here, only the effect of the surface topography (φ_{topo}) has been considered, that is, no tilt and rotation errors and phase noise errors have been included. The interferences that appear between the specimen and the reference mirror are shown in the x- and y-directions. Figure 2A shows the simulation with the smaller

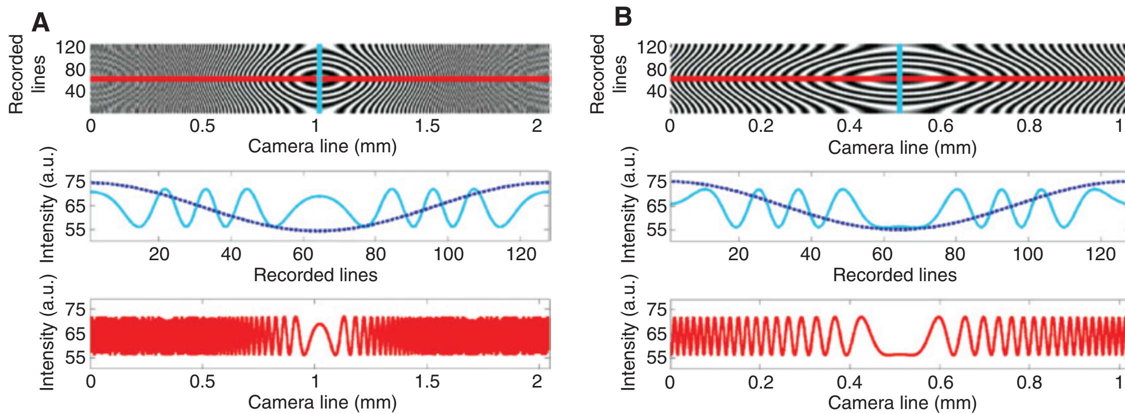

Figure 2: Simulation of the interference fringes of an asphere with different magnifications of the microscope objective. The profile along the x-axis is shown in red, and the profile along the y-axis is light blue. The dotted blue line symbolizes the oscillation $z(t)$ from Eq. (1): (A) results with 5× magnification and a field of view of 2 mm and (B) results with 10× magnification and a field of view of 1 mm.

magnification where a high fringe density is obtained at the end of the camera line. In the simulation shown here, the interference amplitude remains constant; however, in practice with the finite pixel size of the detector, the high fringe frequency could not be resolved, making it difficult to extract the topography. At higher magnification, the fringe density is reduced, which can thus be resolved by the sensor, and then the reconstruction of the topography is possible.

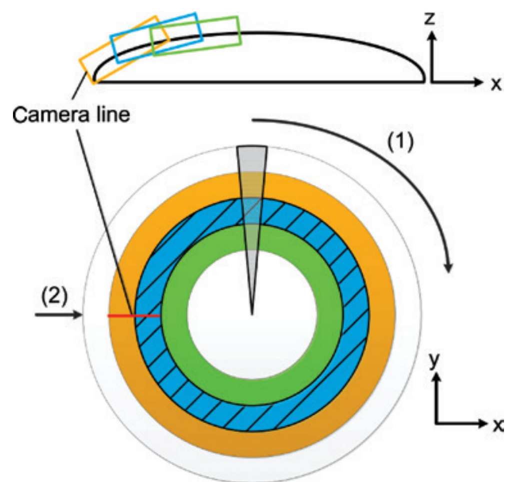

Figure 3: Circular rings on the specimen measured by the line sensor using the rotation axis (1) and the radial axis (2). Boundary conditions for the measurement and stitching process: first boundary condition, the height values have to be the same in a certain overlap region (dotted area); second boundary condition, the height values have to be the same in the radial overlap region (blue striped area).

4 Measurement procedure

The camera line is positioned with respect to the radial direction of the specimen in the x-direction (see Figure 3A). The scanning process starts at the outer boundary of the specimen, resulting in a first ring subaperture. To test the quality of the measured data, we perform the rotational scan by more than a full rotation to achieve a certain overlap region where the same measurement data are expected. Following this, the sensor is moved in the radial direction by half of the length of the camera line (~1 mm), obtaining an overlap of 50%. This is repeated until the whole specimen has been scanned.

In the case of plane mirrors, the only axis needed for the tracking process is the x-axis of the movement system. For the measurement of concave or convex specimens, the sensor has to be moved in additional directions to follow the shape of the specimen and to ensure that the optical axis of the sensor is almost perpendicular to the surface of the specimen. To perform these movements adequately, two additional pieces of information have to be known: an approximate prior knowledge of the geometry of the specimen (accuracy needed: <10 μm) and the absolute distance between the specimen and the sensor. A prior knowledge of the specimen geometry can, in many cases, be obtained with sufficient accuracy from the design data of the specimen. If adequate prior knowledge of the rough surface form is not available, additional measurements are needed. In our case, we used a chromatic-confocal point sensor mounted on a conventional coordinate measuring machine. The second piece of information is the absolute distance between the surface and the sensor, which is additionally needed to calculate in advance the necessary movement of the sensor. This distance is determined using a triangulation procedure where the sensor is

positioned perpendicularly to the surface at two different positions [14].

With the x_b axis (see Figure 1B), the sensor is refocused to ensure an optimal distance between the sensor and the specimen, that is, resulting in a maximum contrast in the interferograms at the center of the line sensor. This focus position is fixed for a whole ring scan and must thus be adequate to cover the height deviations present during a scan.

5 Data evaluation

The signal evaluation process is shown in Figure 4. The interference fringes $I(t)$ are evaluated with a fast Fourier transform (FFT) and a phase evaluation at the dominant frequency [18]. These phase values are corrected because of the ambiguity of the arc-tan function [1]. The unwrapped values are scaled into height values.

The idea of the stitching is to match the measured topographies in the overlap regions of the rings [12]. Two boundary conditions have to be fulfilled to obtain the complete form. The first condition is that, after a rotation of 360°, the same height values should result for this region again (see Figure 3). Normally, this condition is met within the signal noise level. Significant deviations point out a mistake during measurement or evaluation. The second boundary condition is that the height values should be the same in the overlap region between two adjacent circular rings (see Figure 3). The possible differences of the measured form in the overlap region caused by imperfect tilt and offset adjustment of the sensor are removed by adapting the tilt and offset of the measured topographies. To this end, each of the two topographies in the overlap region is fitted by a plane. The second one of these planes is shifted and tilted until both planes agree. These shift and tilt parameters are then used to shift and tilt each topography point. After matching the two topographies, the mean of both values is taken. To avoid parabolic errors in the stitching process, the specimen is measured by several rings. From ring to ring, the sensor is moved stepwise in the x-direction (see Figure 3) from the left boundary to the right boundary of the specimen. Thus, the specimen is scanned twice and this information is used to correct the main axis error.

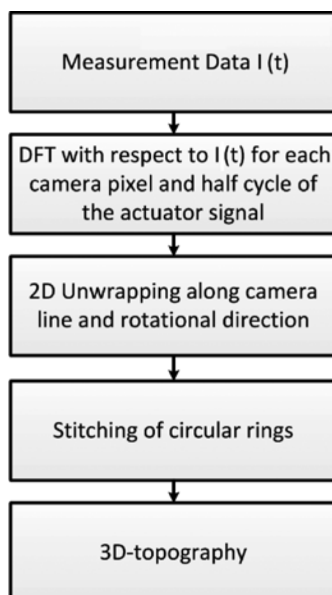

Figure 4: Flow chart of the evaluation process from the measurement data to the stitched 3D topography.

6 Measurement examples

6.1 Stability and reproducibility

The stability of the system was tested by measuring one ring 200 times. Each of these measurements consisted of a standstill of the system for 5 s, a rotation by 370° of the rotation axis c, and again a standstill of the system. The data measured in standstill condition (the axes are switched on but not moving), the median topography along the camera line, and the standard deviation for each pixel were determined. Figure 5A shows the median topography and the standard deviation measured during a standstill period of 5 s (300 single measurements). The height values of the pixels differ due to the topography of the specimen. The standard deviation alone (topography removed) is shown in Figure 5B as a tolerance band. The individual measured topography values have a standard deviation of about 2 nm, which presumably stems from mechanical noise.

Averaging a number of measurements reduces the 2 nm standard deviation. Figure 6 shows the standard deviation of the averaged topography as a function of the number of measurements. The curve follows – in good agreement – the theoretical 1/n behavior here proved up to at least 200 individual topography measurements. This measurement run took about 6 h, demonstrating the good long-term stability of our system.

Each pixel yields a circular line topography of the specimen. Hence, using 25 rotations gives 25 topography measurements that should agree. The median topography calculated using the results of these 25 rotations

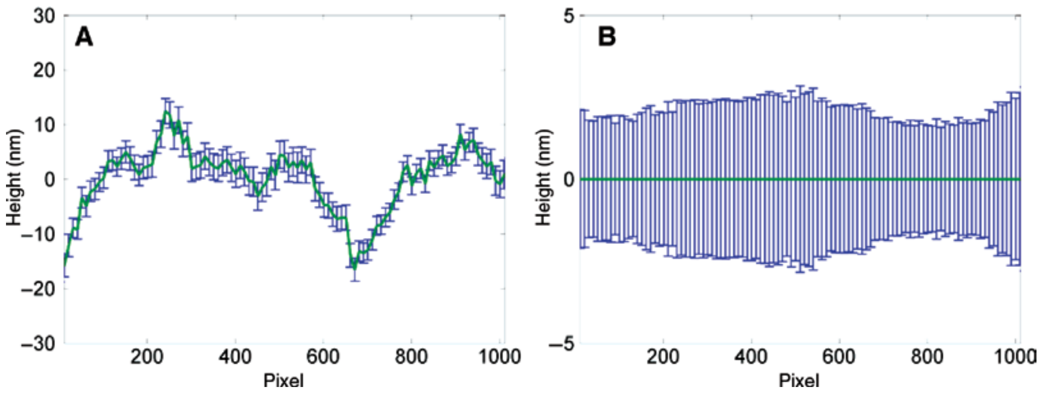

Figure 5: (A) Measurement result, all axes are switched on, the median topography of 300 measured lines, and its standard deviation is plotted. (B) Standard deviation after subtracting the mean value.

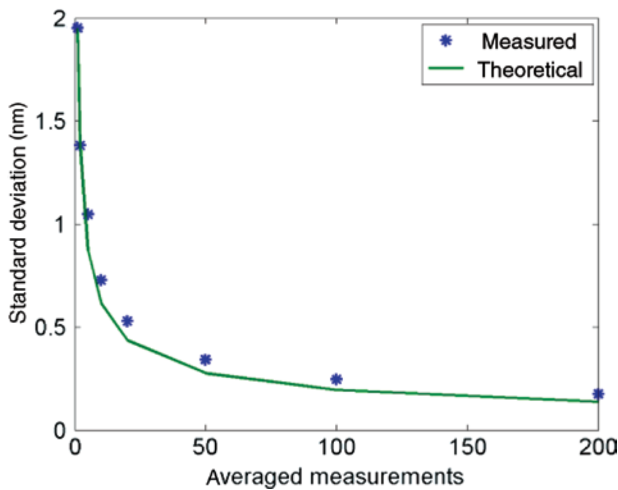

Figure 6: Standard deviation of measurement results after averaging: measured values (blue stars) and theoretical limit (green line).

is presented in Figure 7A. The standard deviation of the measurements for this pixel (median topography subtracted) is shown in Figure 7B. The standard deviation (14 nm) is considerably larger than in the standstill case because of errors of the rotation axis c.

6.2 Example measurement of a sphere

Figure 8A presents the topography of a sphere (design radius: 250 mm, diameter: 25.4 mm) measured with only one (fixed) camera position. The best fit radius obtained from the measured topography is 250.143 mm. After subtracting this, the residuals shown in Figure 8B remain. The standard deviation of the residuals is 3.7 nm, which is larger than expected from the standstill measurements (2 nm), possibly resulting from the real topography.

The full 3D topography of this sphere was measured using the rotation and stitching procedure. In total, 25 circular rings were stitched together. In Figure 9A and B, only a few rings are shown for the better visibility of the stitching process. The final result is shown in Figure 9C. Subtracting the best fit sphere of the stitched topography

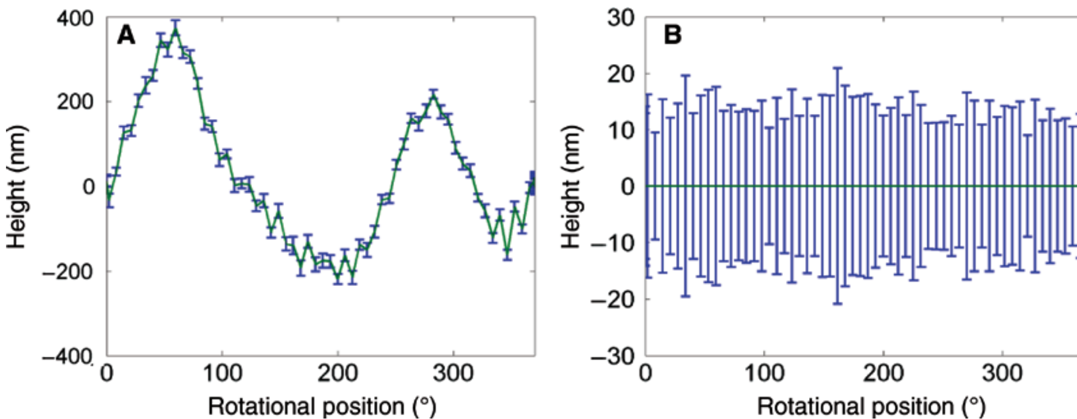

Figure 7: (A) Height change for a single sensor pixel during 25 measurements (green) starting at 0° and stopping at 370° and its standard deviation (blue). (B) Same as (A), but the topography is subtracted.

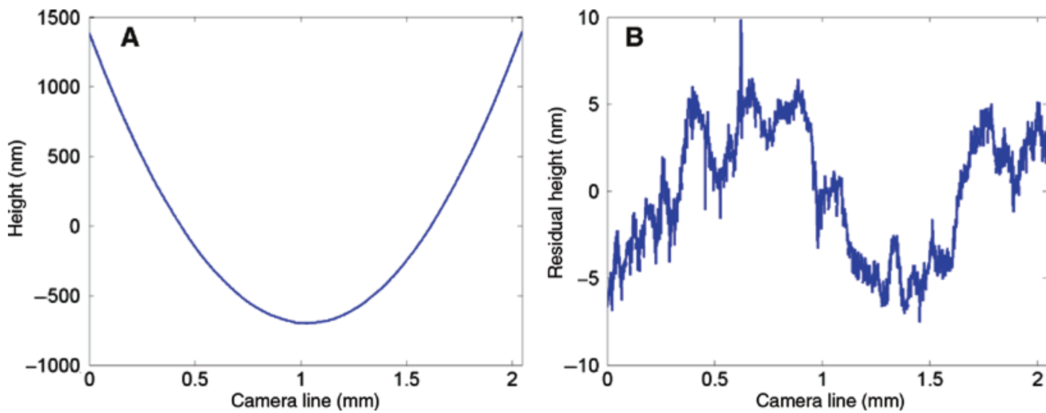

Figure 8: (A) Measurement result of one camera line and (B) residuals when the best-fit radius of 250.143 mm is subtracted from the height values.

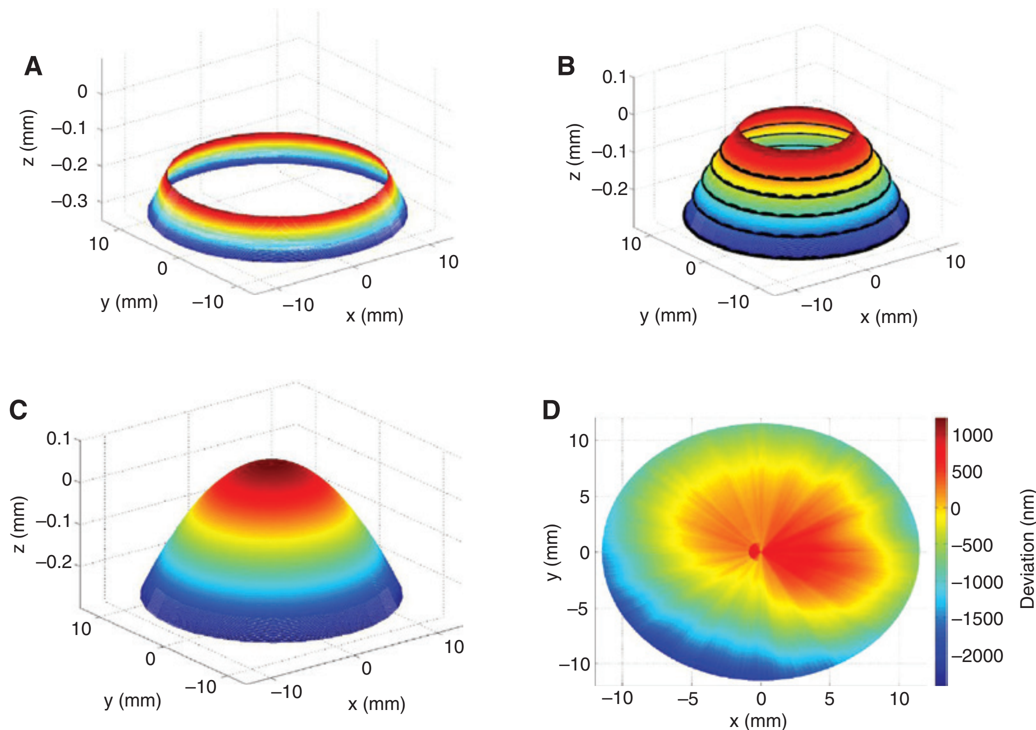

Figure 9: Measurement of a spherical lens demonstrating the stitching procedure: (A and B) black lines denote the boundary lines between two consecutive rings and (C) whole topography using all measured rings and (D) deviation from the perfect design.

yields to a deviation from the perfect design of a sphere (see Figure 9D). This is a preliminary measurement result that will be improved by better calibration procedures in the future.

7 Outlook

Because the system is scalable and flexible, it can be used for many differently shaped specimens, ranging from planes and spheres to aspheres. The measurement system can be set up for a moderate price; thus, it may be of interest for the precision measurement and engineering sectors. The minimal radius of curvature of the specimen that is measurable can be decreased if microscope objectives with higher magnifications are used and/or if only the central parts of the camera line are evaluated. In the extreme case, only one sensor pixel of the line sensor can be used (making it a point sensor), which would allow steep aspheres to be measured. In principle, the sensor

could be moved also in the radial direction during the measurement, which would enable the measurement of specimens without any prior knowledge. The next steps of our work will be to measure the tilt error of the rotation axis of the specimen, to improve the stitching process with a parallel stitching procedure, to compare the form measurement results with other instruments, and to estimate the achieved measurement uncertainty.

Acknowledgments: The financial support of this research work (LE 992/7-2, EH 400/4-2) by the Deutsche Forschungsgemeinschaft (DFG) is gratefully acknowledged.

References

[1] D. Malacara, Optical Shop Testing (Wiley-Interscience, John Wiley & Sons, Inc., 2007).
[2] M. Salleh, Q. Yang, and B. Jones, Finite Element Modeling and Simulation of Probe System, IMTC 2005 – Instrumentation and Measurement Technology Conference, Ottawa, Canada, 17–19 May 2005.
[3] F. Meli and A. Küng, Meas. Sci. Technol. 18, 074007 (2006).
[4] G. Berger and J. Petter, Techn. Mess. 81, 2–7 (2014).
[5] P. de Groot, Adv. Opt. Photon. 7, 1–65 (2015).
[6] D. Malacara, M. Servin and Z. Malacara, Interferogram Analysis for Optical Testing (CRC Press, Taylor & Francis Group, Boca Raton, FL, 2005).
[7] J. Millerd, N. Brock, J. Hayes, M. North-Morris, M. Novak, et al., Proc. SPIE 5531, 304–314 (2004).
[8] A. Hettwer, J. Kranz, J. Schwider, Opt. Eng. 39, 960–966 (2000).
[9] R. Castonguay and P. Swaykowski, Scanning simultaneous phase-shifting, USPO #7,561,279 (2009).
[10] S. O. Donohue, P. Murphy, J. Fleig and G. Devries, Stitching interferometry for flexible asphere metrology, 21st ASPE Annual Meeting, ASPE Proceedings (2006).
[11] H. Knell, S. Laubach. G. Ehret and P. Lehmann, Opt. Express 22, 29787–29789 (2014).
[12] S. Laubach, G. Ehret, H. Knell and P. Kühnhold, P. Lehmann. In: DGaO Proceedings, (2014). Available at: http://www.dgao-proceedings.de. ISSN: 1614-8436.
[13] H. Knell, M. Schake, M. Schulz and P. Lehmann, Proc. SPIE 9132, 91320I (2014).
[14] S. Laubach, G. Ehret, H. Knell and P. Kühnhold, P. Lehmann. In: DGaO Proceedings, (2015). Available at: http://www.dgao-proceedings.de. ISSN: 1614-8436.
[15] O. Sasaki and H. Okazaki, Appl. Opt. 25, 3137–3140 (1986).
[16] O. Sasaki and H. Okazaki, Appl. Opt. 25, 3152–3158 (1986).
[17] M. Takeda, H. Ina and S. Kobayashi, J. Opt. Soc. Am. 72, 156–160 (1982).
[18] H. Knell and P. Lehmann, Proc. SPIE 8788, 87880R (2013).